01 Dec 2012

Fabrication of CaO-NaO-SiO2/TiO2 Scaffolds for Surgical Applications

A. W. Wren

A. Coughlan

K. E. Smale

S. T. Misture

et. al. For a complete list of authors, see https://scholarsmine.mst.edu/che_bioeng_facwork/1151

Recommended Citation

Fabrication of CaO–NaO–SiO$_2$/TiO$_2$ scaffolds for surgical applications

A. W. Wren · A. Coughlan · K. E. Smale ·
S. T. Misture · B. P. Mahon · O. M. Clarkin ·
M. R. Towler

Abstract A series of titanium (Ti) based glasses were formulated (0.62 SiO$_2$–0.14 Na$_2$O–0.24 CaO, with 0.05 mol% TiO$_2$ substitutions for SiO$_2$) to develop glass/ceramic scaffolds for bone augmentation. Glasses were initially characterised using X-ray diffraction (XRD) and particle size analysis, where the starting materials were amorphous with 4.5 μm particles. Hot stage microscopy and high temperature XRD were used to determine the sintering temperature ($\sim$700 °C) and any crystalline phases present in this region (Na$_2$Ca$_3$Si$_6$O$_{16}$, combeite and quartz). Hardness testing revealed that the Ti-free control (ScC—2.4 GPa) had a significantly lower hardness than the Ti-containing materials (Sc1 and Sc2 $\sim$6.6 GPa). Optical microscopy determined pore sizes ranging from 544 to 955 μm. X-ray microtomography calculated porosity from 87 to 93 % and surface area measurements ranging from 2.5 to 3.3 SA/mm^3. Cytotoxicity testing (using mesenchymal stem cells) revealed that all materials encouraged cell proliferation, particularly the higher Ti-containing scaffolds over 24–72 h.

A. W. Wren (✉) · A. Coughlan · K. E. Smale ·
S. T. Misture · M. R. Towler
Inamori School of Engineering, Alfred University, Alfred,
NY 14802, USA
e-mail: wren@alfred.edu

B. P. Mahon
Institute of Immunology, National University of Ireland,
Maynooth, Co. Kildare, Ireland

O. M. Clarkin
South Eastern Applied Materials Research Centre, Waterford
Institute of Technology, Waterford, Ireland

M. R. Towler
Materials & Surface Science Institute, University of Limerick,
Limerick, Ireland

1 Introduction

Mesoporous materials have generated considerable interest in recent years for medical applications, such as controlled drug delivery and synthesis of novel nanomaterials. This is due to attractive features such as high surface area, uniform pore size and high pore volume [1]. Highly porous materials such as Santa Barbara amorphous type materials (SBA-15) and mobil crystalline materials (MCM-41) have been successfully used in drug delivery systems as it is possible for them to adsorb and release drug molecules from the meso-structured matrices at a controlled rate, however, due to the low bioactivity attributed to pure silica, their use as bone repair substitutes is limited [1]. More recently focus has turned to using bioactive glasses and glass–ceramic materials for medical applications, in particular as bone substitutes and scaffolds. 3D porous scaffolds are preferential to using traditional particulates or granules in treating large bony defects as they provide an interconnected network which permits hosts cell migration, nutrient delivery, bone ingrowth and eventually vascularization [2, 3].

Some specific attributes required for an ideal scaffold, as suggested by Boccaccini et al. include the ability to deliver cells to the wound site, excellent osteoconductivity, biodegradability, appropriate mechanical strength, high porosity (>90 %) and pore size >400–500 μm. Bioactive glasses meet a number of these criteria (excellent osteoconductivity and bioactivity, ability to deliver cells and controllable biodegradability) which makes bioactive glasses an attractive group of materials as scaffolds for tissue engineering [3–5].

Studies on glass–ceramic scaffolds derived from Hench's 45S5 Bioglass have shown to exhibit appropriate mechanical stability, tailorable bioresorbability and excellent bone-bonding capability due to the formation of a hydroxyapatite surface layer [1, 3, 5, 6]. Their osteogenic behaviour is thought to be due to the release of specific concentrations of ions that stimulates osteogenic cells resulting in bone growth [5]. Other materials such as apatite-wollastonite bioactive glass–ceramic (AW–GC) have been investigated due to good bioactivity, biodegradability and osteoinductivity [7], and also polylactic acid/calcium phosphate glass scaffolds, which are completely degradable [8].

The work herein sees the characterisation and development of CaO–Na$_2$O–SiO$_2$/TiO$_2$ based glass–ceramic scaffolds. Previous work on glasses with similar compositions determined TiO$_2$ to act as a network modifying cation [9], and as such, its substitution for SiO$_2$ in this instance may result in a more biodegradable scaffold. Titanium (Ti) was used as it has been widely used in the field of orthopaedics and has exhibited positive tissue response in commercial biomaterials [10–12]. Ti has been used for developing craniofacial prosthetics, and ossicular implants [11]. Ti6Al4V implants, Ti–N coatings, K$_2$O–SiO$_2$–TiO$_2$ glasses and Ti-gels have all reported the growth of a CaP surface layer when tested in simulated body fluid (SBF) [13–16], which is reportedly due to a naturally occurring oxide surface layer which forms Ti–OH$^-$, which in turn, favours precipitation of Ca and P ions when tested in SBF [13, 16, 17].

This study investigates the substitution of TiO$_2$ for SiO$_2$ in the glass phase of the starting materials and its effect on the structural, mechanical and biological properties. Scaffolds were produced by an existing polymer-sponge method [4], however, a heat treatment profile for the starting glasses was derived using both hot stage microscopy (HSM) and high temperature X-ray diffraction (HT-XRD).

2 Materials and methods

2.1 Material fabrication

2.1.1 Glass melting

Three glass compositions were formulated for this study. The SiO$_2$ content of the glass was substituted by TiO$_2$ throughout the series, Sc1 and Sc2 (Table 1). A Ti-free glass was used as a control (ScC) for comparison. Glasses were prepared by weighing out appropriate amounts of analytical grade reagents (Fisher Scientific, Pittsburg PA, USA) and ball milling (1 h). The powdered mixes were oven dried (100 °C, 1 h) and fired (1,500 °C, 1 h) in platinum crucibles and shock quenched in water. The resulting frits were dried,

ground and sieved to retrieve glass powders with a particle size less than 25 μm.

2.1.2 Glass scaffold production

Scaffolds were produced with each glass formulation denoted ScC, Sc1 and Sc2, where Sc2 contains the highest concentration of TiO$_2$. Polyvinyl alcohol (PVA, 0.008 g) was initially dissolved in 9.3 ml of de-ionised water for 1 h and heated to 55 °C. 12 g of glass powder was added to each flask and stirred for 1 h. 10 mm × 8 mmϕ cylindrical polyurethane foams were cut and immersed in the glass slurry, stirred with a spatula to ensure all pores were filled within the slurry. After approximately 10 min the glass embedded foam was allowed dry on a foam bed for 24 h. The scaffolds were then heat treated in a furnace to remove the foam and sinter the suspended glass particles. Figure 1 shows a schematic of the foam production process and subsequent testing of the scaffolds.

2.1.3 Heat treatment profile

Heat treatment of the glass/ceramic scaffolds was determined using HSM and HT-XRD. The temperature profile consists of heating the scaffolds at a rate of 10 °C/min to the sintering temperature and holding for 5 h. The scaffolds were then heated to the sintering temperature +40 °C at a rate of 1 °C/min and then held for 5 h. The scaffolds were then cooled slowly to room temperature at a rate of 5 °C/min (Fig. 2).

2.2 Glass characterisation

2.2.1 XRD

Diffraction patterns were collected using a Siemens D5000 X-ray Diffraction Unit (Bruker AXS Inc., WI, USA). Glass powder samples were packed into standard stainless steel sample holders. A generator voltage of 40 kV and a tube current of 30 mA was employed. Diffractograms were collected in the range $10° < 2\theta < 80°$, at a scan step size 0.02° and a step time of 10 s. Any crystalline phases present were identified using Joint Committee for Powder Diffraction Studies (JCPDS) standard diffraction patterns.

Table 1 Glass formulations (mol. Fr.)

	ScC	Sc1	Sc2
SiO$_2$	0.62	0.57	0.52
TiO$_2$	0.00	0.05	0.10
Na$_2$O	0.14	0.14	0.14
CaO	0.24	0.24	0.24

Fig. 1 Flow chart for scaffold fabrication and testing

a.) Glass Production

Sc-Control
Sc$_1$ & Sc$_2$

b.) Glass Characterization

XRD, DTA, NC, PSA

c.) Sintering Profile

HSM, High Temp. XRD

d.) Scaffold Fabrication

Glass Powder
+ PVA + H$_2$O

Spinning (3hrs)

Dried (24 hrs)

Furnace (Heat Treatment)

e.) Imaging & Composition

Electron Microscopy + EDS
CT Microtomography

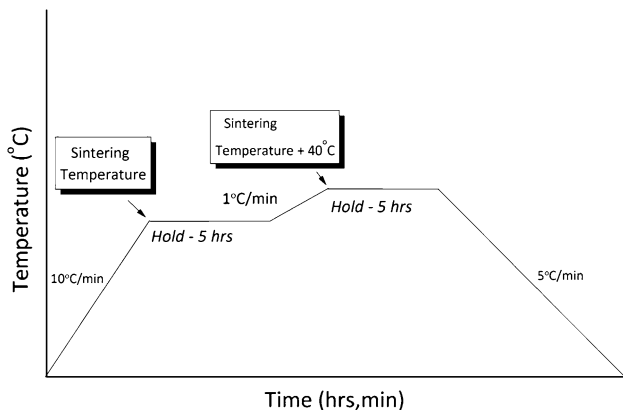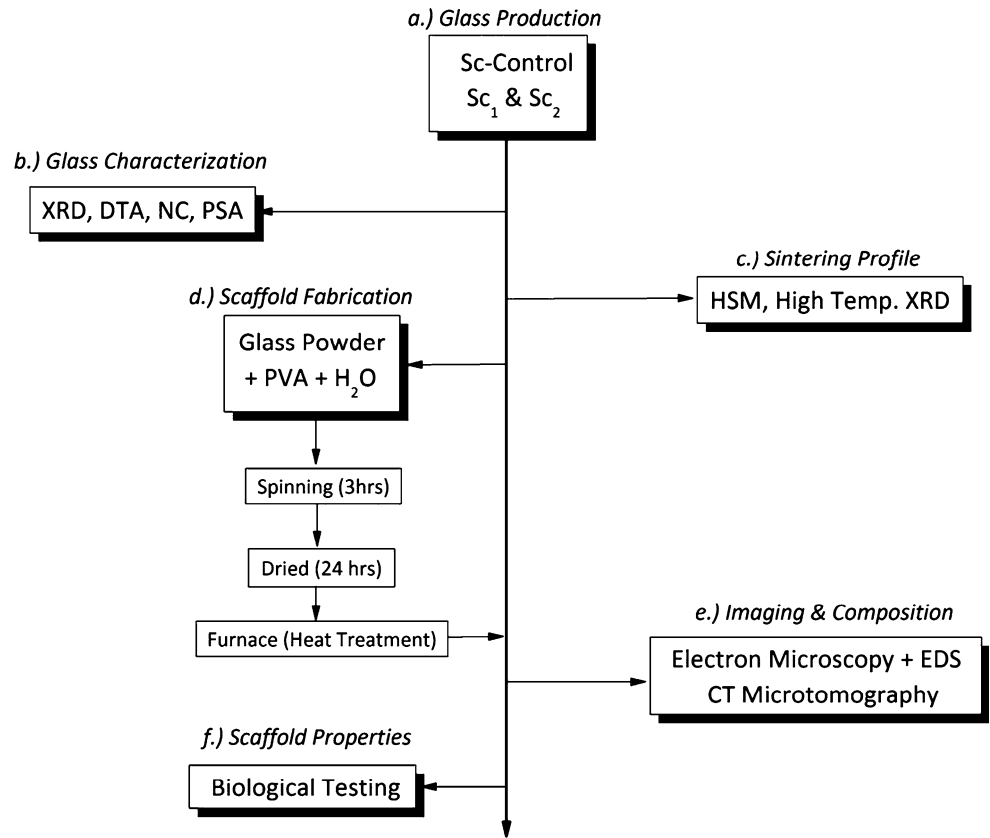*f.) Scaffold Properties*

Biological Testing

Fig. 2 Sintering profile used for scaffolds

2.2.2 Network connectivity

The network connectivity (NC) of the glasses was calculated with Eq. 1 using the molar compositions of the glass. NC calculations were performed assuming that Ti performs as a network former and also as a network modifier.

$$NC = \frac{No.BOs - No.NBOs}{Total\,No.\,Bridging\,Species} \qquad (1)$$

where *NC* network connectivity, *BO* bridging oxygens and *NBO* non-bridging oxygens.

2.2.3 Differential thermal analysis (DTA)

A combined differential thermal analyer/differential thermal calorimeter (DSC, Q10-DSC, TA Instrumental Inc., New Castle, DE) was used to measure the glass transition temperature (T_g) for each glass. A heating rate of 20 °C/min was used in a nitrogen atmosphere up to a maximum temperature of 700 °C, using a blank reference in a matched platinum crucible.

2.2.4 Particle size analysis (PSA)

Particle size analysis (PSA) was achieved using a Beckman Coulter Multisizer 4 Particle size analyser (Beckman-Coulter, Fullerton, C.A, USA). The glass powder samples were evaluated in the range of 0.4–100.0 μm and the run length took 60 s. The fluid used was water and was used at a temperature range between 10 and 37 °C. The relevant volume statistics were calculated on each glass.

2.2.5 HSM

A MISURA side view hot stage microscope (HSM), Expert Systems (Modena, Italy), with image analysis system and electrical furnace, with max temperature of 1,600 °C and max rate of 80 °C/min. The parameters for this experiment

were a heat rate of 20 °C/min from 20 to 500 °C and 5 °C/min from 500 to 1,200 °C. The computerised image analysis system automatically records and analyses the sample geometry during heating.

2.2.6 HT-XRD

Powders were analysed using a custom high temperature XRD furnace using a Siemens D5000 XRD unit with a Vantec1 linear position-sensitive detector [18]. Cu Kα radiation was used, and measurements were collected over an angular range of 10–70° 2θ with scan rate of 2.25°/min. Patterns were measured at RT and from 400 to 800 °C in steps of 20 °C. Samples were heated at a rate of 20 °C/min and then cooled at 60 °C/min. All measurements were performed in static air.

2.3 Hardness testing

Hardness testing was completed on discs ($8\phi \times 2$ mm) sintered using the same heat treatment profile as the scaffolds, where 10 measurements were taken on each disc and three discs were used for each material (total $n = 30$/sample). A Shimadzu HMV-2000 hardness testing machine was used with a 500 g load cell with 15 s intervals.

2.4 Scaffold analysis

2.4.1 Scanning electron microscopy and energy dispersive X-ray analysis (SEM–EDS)

Backscattered electron (BSE) imaging was carried out with an FEI Co. Quanta 200F Environmental Scanning Electron Microscope. Additional compositional analysis was performed with an EDAX Genesis Energy-Dispersive Spectrometer (EDS). All EDS spectra was collected at 20 kV using a beam current of 26 nA. Quantitative EDS spectra was subsequently converted into relative concentration data.

2.4.2 Optical microscopy

Estimation of pore size was conducted using an Olympus IX20-UCB Optical Fluorescent Microscope at 4× magnification. Mean pore size was calculated by measuring the diameter of (1) starting polyurethane scaffolds, (2) ScC, (3) Sc-1 and (4) Sc-2. 10 pores were measured from three different scaffolds (total $n = 30$) for each material and the mean and standard deviation was calculated. The software used to measure the pore size was Image-Pro AMS 5.1 where a 100 μm calibration standard was used for accuracy.

2.4.3 X-ray microtomography

The porous scaffold samples were examined using a Phoenix Nanotom™ X-ray microtomography system (GE Sensing and Inspecting Technologies, Boston, USA). The X-ray source was molybdenum, to which a current of 160 μA Amps and a voltage of 70 kV was applied. 360 radiographs were collected through a rotation of 0–360° without the use of filters. Radiographs were collected using a 2 megapixel high contrast flat panel digital detector with three frame averages per acquired radiograph, skipping the first acquisition (to prevent vibration). Volumetric reconstruction was carried out using datosIX—reconstruction software (GE Sensing and Inspecting Technologies). During the image reconstruction process, the beam hardening correction parameter was set to 50 %. The porosity and surface area were calculated and analysed using Volume graphics studio™ software by extracting a volumetric region of interest (ROI) and analysing that volume for % filled space and total surface area. From this information, porosity (%) and surface area/mm³ was determined.

2.5 Stem-cell culture analysis

Murine mesenchymal stem cells from transgenic DsRed mice which constitutively express a red fluorescent protein [19] were obtained as previously described [20]. Cells were cultured in Mesencult basal medium, supplemented with 10 % (v/v) Mesencult supplement (Stem Cell Technologies, Vancouver, Canada) and used at low passage (<10) [20]. MSC expressed CD90 and CD105 but not CD34, CD45 or MHC class II, and possessed tri-lineage differentiation potential [21]. Procedures were approved by the research ethics committee of the National University of Ireland, Maynooth. Scaffolds were sterilized by autoclaving at 120 °C for 20 min and stored overnight in complete culture medium. All activities were performed aseptically and all incubations performed at 37 °C in a humidified 5 % CO_2 atmosphere. Scaffolds were washed twice in sterile PBS, and placed in sterile polystyrene Petri dishes (NalgeNunc International, Rochester, NY). To each scaffold, 200 μl of MSC at 2×10^5 cells/ml were carefully distributed, allowing all of the seeding culture to enter the scaffold; this was cultured for 2 h to allow MSC adherence. At the end of this period, scaffolds to which MSC had adhered, were removed and cultured in 1 ml of fresh culture medium in 24 well tissue culture plates (NalgeNunc International), such that scaffolds were completely submerged. Scaffolds were examined by epi-fluorescent microscopy. MSC proliferation was determined by WST-1 assay (Roche Diagnostics, Indianapolis, USA) according to the manufacturer's instructions.

2.6 Statistical analysis

One-way analysis of variance (ANOVA) was employed to compare means where applicable. Comparison of relevant means was performed using the post hoc Bonferroni test. Differences between groups was deemed significant when $P \leq 0.05$. Statistical analysis was performed using SPSS software for windows version 16 (SPSS Inc. Chicago, IL).

3 Results and discussion

The starting materials developed for this study were CaO–Na$_2$O–SiO$_2$ based glasses (*ScC*) and the Ti substituted experimental glasses, *Sc1* and *Sc2*. Initially XRD was undertaken to ensure that each starting material was amorphous prior to heat treatment (Fig. 3a). PSA was also conducted in order to determine the mean particle size and distribution post-grinding and sieving. Figure 3b shows that there is no significant change in particle size between materials and the size ranged from 4.65 μm (*ScC*), 4.61 μm (*Sc1*) to 4.36 μm (*Sc2*). Smaller particle sizes are preferential for sintering and particle sizes of <5 μm have previously been used for fabrication of Bioglass based scaffolds [22].

Network connectivity (NC) calculations were carried out to theoretically determine the structural role played by TiO$_2$ as it substitutes SiO$_2$ in the glass network. Assuming TiO$_2$ performs as a network modifier, the NC decreases from 2.77 (*ScC*) to 2.49 (*Sc1*) to 2.15 (*Sc2*). Thermal

analysis of each glass revealed no significant change in glass transition temperature (T_g) between *ScC* (606 °C) and *Sc1* (611 °C), however, *Sc2* reduced slightly to 596 °C. This slight reduction in T_g may be attributed to de-polymerisation of Si–O–Si glass network as indicated by the reduction in NC as has been previously determined by the authors [9]. It may also be the case that the relatively low substitution of TiO$_2$ for SiO$_2$ results in a relatively insignificant change in T_g (Fig. 4).

To determine the sintering temperature of each glass, HSM was employed. HSM determined that the sintering temperature of each material was similar considering the control *ScC*—695 °C, *Sc1*—707 °C and *Sc2*—695 °C. The addition of TiO$_2$ was also found to reduce the melt temperature (*Sc1*, *Sc2*—1,107 °C) when compared to the control (*ScC*—1,146 °C) which is also indicative of a de-polymerised silicate glass network. In order to determine any mechanical differences attributed to TiO$_2$, hardness testing was performed on sintered discs produced from each glass, *ScC*, *Sc1* and *Sc2*. Results determined *ScC* to have a much lower hardness value than either of the Ti containing samples. *ScC* hardness was found to be 2.4 GPa which was significantly lower than both *Sc1* (7.1 GPa, $P = 0.0001$) and *Sc2* (6.1 GPa, $P = 0.0001$), suggesting that the inclusion of TiO$_2$ results in a more interconnected glass/ceramic structure post-sintering. At present porous scaffolds are suitable as grafts for low-load sites subjected to compression only, such as fused spinal vertebrae [23]. In this case the mechanical strength of the materials can be achieved during processing by altering the starting composition (Fig. 5).
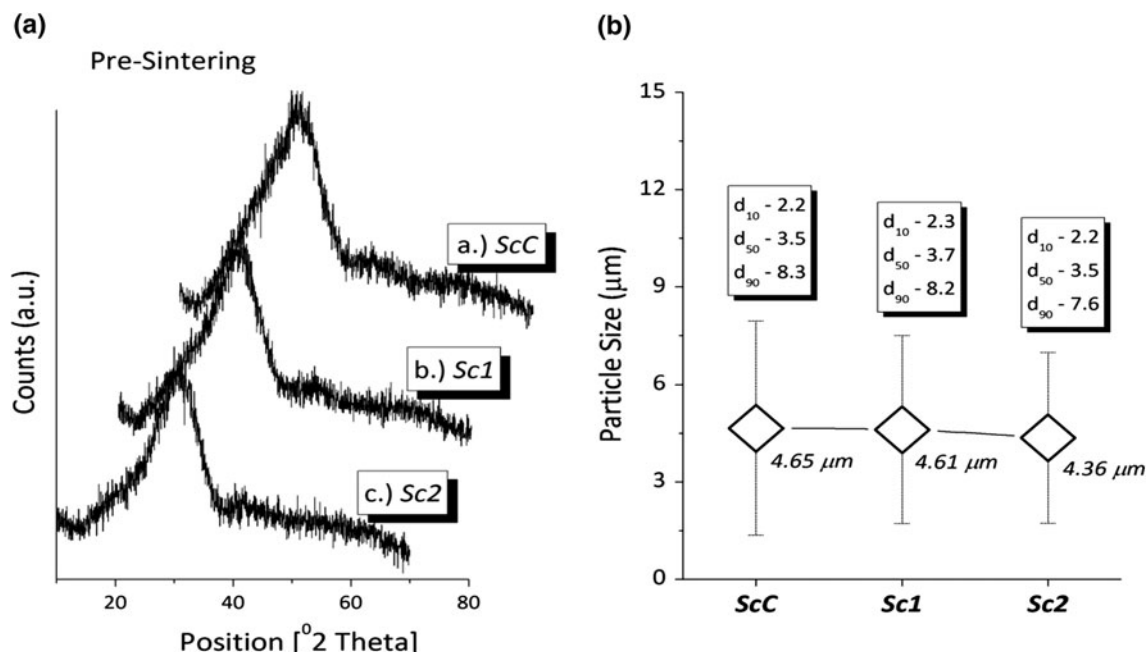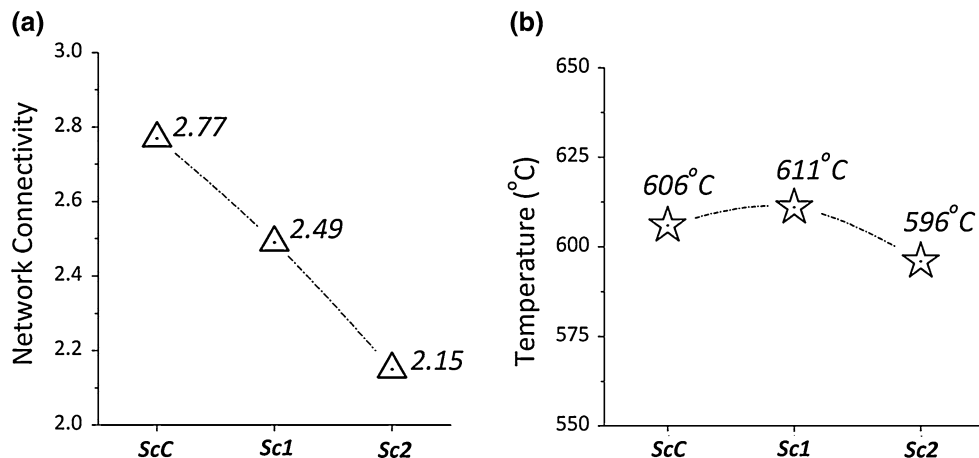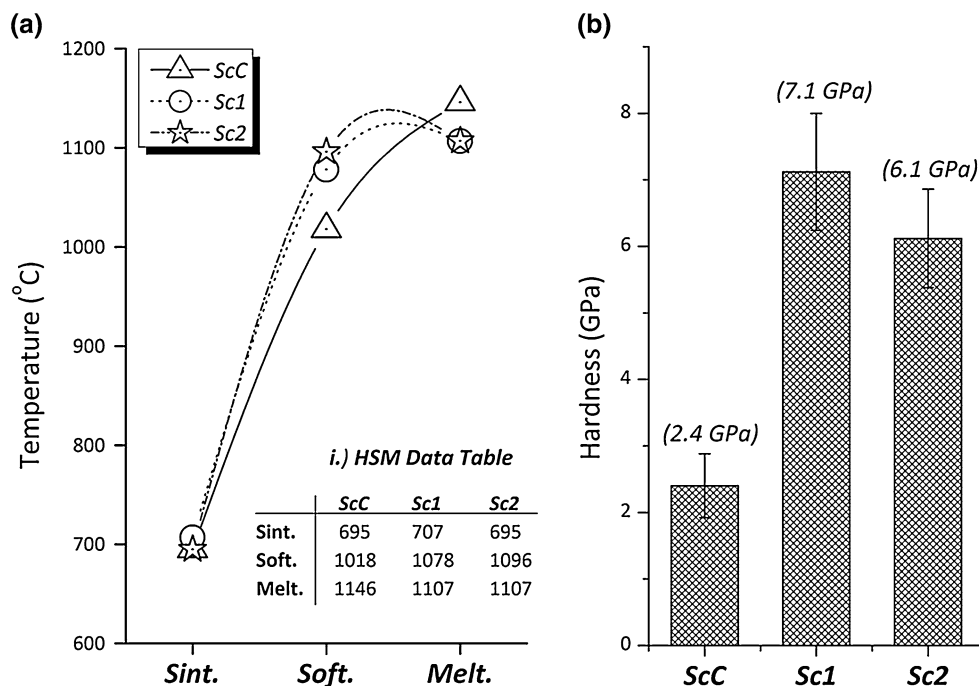

Fig. 3 **a** XRD scans of initial glass series, **b** particle size of glass series

Fig. 4 a Network connectivity and **b** T_g of glass series

Fig. 5 a Hot stage microscopy and **b** hardness testing of glass series

i.) HSM Data Table	ScC	Sc1	Sc2
Sint.	695	707	695
Soft.	1018	1078	1096
Melt.	1146	1107	1107

A possible explanation for the different mechanical properties when comparing the Ti scaffolds to the Ti-free scaffolds, may be the reduction in Si–O–Si bonds in the Ti-containing materials. As these bonds decrease with the addition of network modifiers, the concentration of non-bridging oxygens (NBOs) increases. This would likely facilitate greater interconnectivity during heat treatment as less thermal energy would be required to decompose the glass structure.

High temperature XRD (HT-XRD) was undertaken to determine the degree of crystallization occurring at the sintering temperature during processing, and also to determine crystal phases present. HT-XRD phase identification revealed $Na_2Ca_3Si_6O_{16}$, combeite ($Na_6Ca_3Si_6O_{18}$) and quartz (SiO_2) phases which were present in each material after cooling. XRD was performed on the ground up scaffolds post-sintering and it was found that at the sintering temperature (700–760 °C), crystal formation was also present. This was particularly evident in the control material (ScC), however, crystal formation was also present in the Ti-containing materials (Sc1 and Sc2), but to a lesser degree. It was observed that as the concentration of TiO_2 increased, the degree of crystallinity was found to reduce to the point where Sc2 partially retained some of its amorphous character, suggesting Ti possible role in inhibiting crystallization. The crystal phases present in the
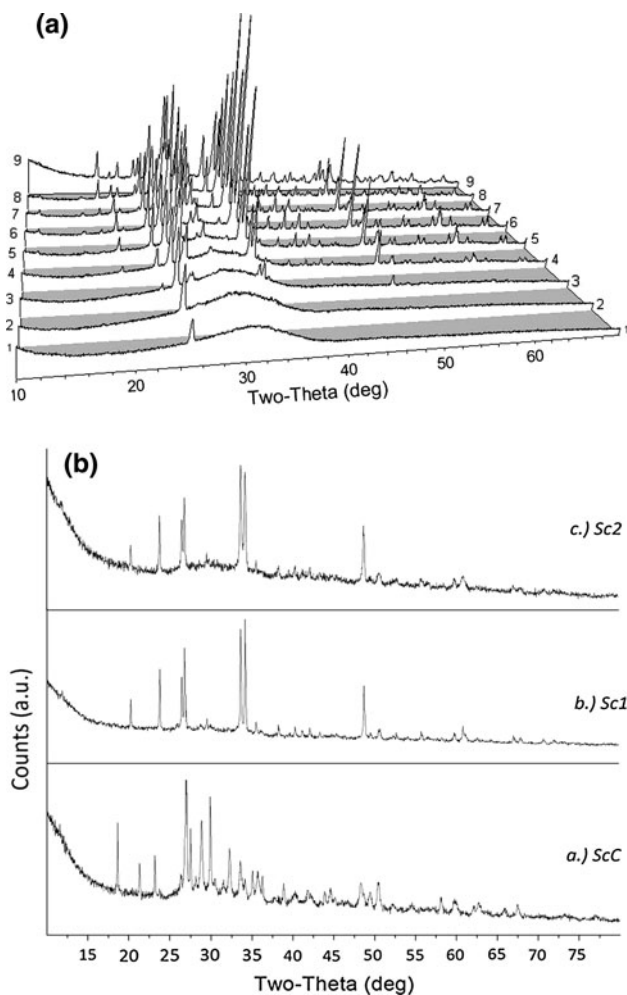
Fig. 6 a HT-XRD scan of *Sc1* forming $Na_2Ca_3Si_6O_{16}$, combeite and quartz phases and **b** XRD of ground up scaffolds post cooling exhibiting predominantly forming $Na_2Ca_3Si_6O_{16}$ phases

ground up scaffolds were found to be predominantly sodium–calcium–silicate ($Na_2Ca_3Si_6O_{16}$) (Fig. 6).

High temperature XRD (HT-XRD) revealed that low-level crystallinity was present at the sintering temperature; however, the characteristic amorphous trace was also retained. As was expected, with an increase in temperature ($\sim$820 °C), the amorphous content from each material was partially converted to exhibit crystalline phases. It has been suggested that the use of porous bioactive glasses as scaffolding materials is limited by their mechanical properties and that the sintering profiles employed to enhance their mechanical properties are performed in a range of temperatures, particularly between 900 and 1,100 °C, causing the glasses (for example Bioglass) to crystallize into a glass/ceramic [24]. Although this fact does not compromise the formation of bone–biomaterial bonding, the HA formation in vitro as well as the bonding process in vivo are slowed down by crystallization and the rate of HA

formation decreases as the percentage of crystallization increases [24]. The low-level of crystallinity presented here at the sintering temperature is favourable as these materials will impart greater bioactivity in vivo due to the therapeutic effect of the glass phase. High sintering temperatures can result in turning bioactive glasses, such as Bioglass 45S5, into inert materials [25].

Glass/ceramic scaffolds were produced according to the temperature profile presented in Fig. 2, and are composed of both amorphous and crystalline phases. Microscopy, both SEM and optical microscopy was employed to investigate the structure of the scaffolds. SEM/EDS was used initially to clarify the absence of Ti in the control scaffold (*ScC*) and to confirm the presence of Ti in *Sc1* and *Sc2*. It was also determined that Ca, Na, Si and O were also present for each material. SEM imaging shows the presence of the porous sintered scaffolds (Fig. 7a), and the sintered surface of *Sc2* showing interlocking of the crystal grains (Fig. 7b). Rough surfaces, as presented in Fig. 7b, can be advantageous in scaffold fabrication as a rough surface is an ideal texture to induce progenitor cell attachment and adsorption of biological metabolites [24].

Optical microscopy (Fig. 8) was used to determine the mean pore diameter of the starting foam, and the sintered glass/ceramic scaffolds (post heat treatment). Measurement of the polymer foam determined a mean pore diameter of 955 μm. Post-coating and sintering the mean pore diameter showed an overall decrease, which was particularly evident with the Ti containing materials. The Ti-free control (*ScC*) exhibited a mean pore diameter of 678 μm, while *Sc1* and *Sc2* showed a significant reduction in pore diameter when compared to the pre-processed polymer, 528 μm ($P = 0.000$) and 544 μm ($P = 0.000$), respectively. This is expected as the polymer burns out, the glass particles densify during the sintering process resulting in a reduced pore diameter. The smaller pore diameter as experienced with *Sc1* and *Sc2* suggests a higher degree of densification than the control *ScC*, however, this difference does not reach statistical significance. The pore diameter determined here correlates well to suggestions by Chen et al. that a pore diameter of $>$400–500 μm is suitable for scaffolds for tissue engineering applications [4, 26, 27] and a pore diameter of at least 100 μm to allow cell migration [26, 28]. It has been reported in the literature that large pores can be very effective in satisfying cell size and migration requirements, however, it has also been cited that micropores ($<$10 μm) are required to promote fluid diffusion [24] and capillary growth [29].

X-ray microtomography was further employed to analyse the porous structure of the scaffolds. Figure 9 shows the X-ray microtomographic images of each scaffold. Figure 9a represents the control scaffolds *ScC*, which have thicker trabecular-like support struts when compared to

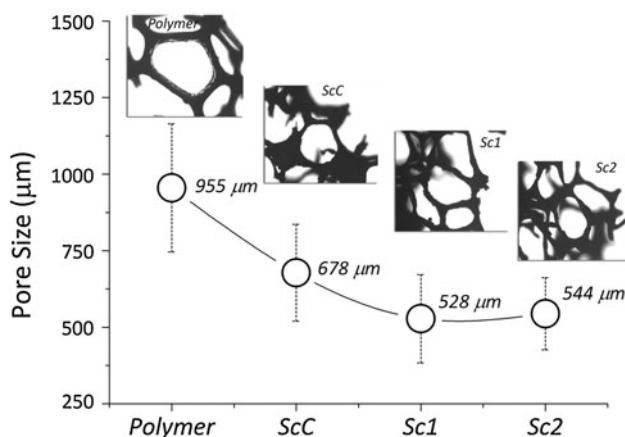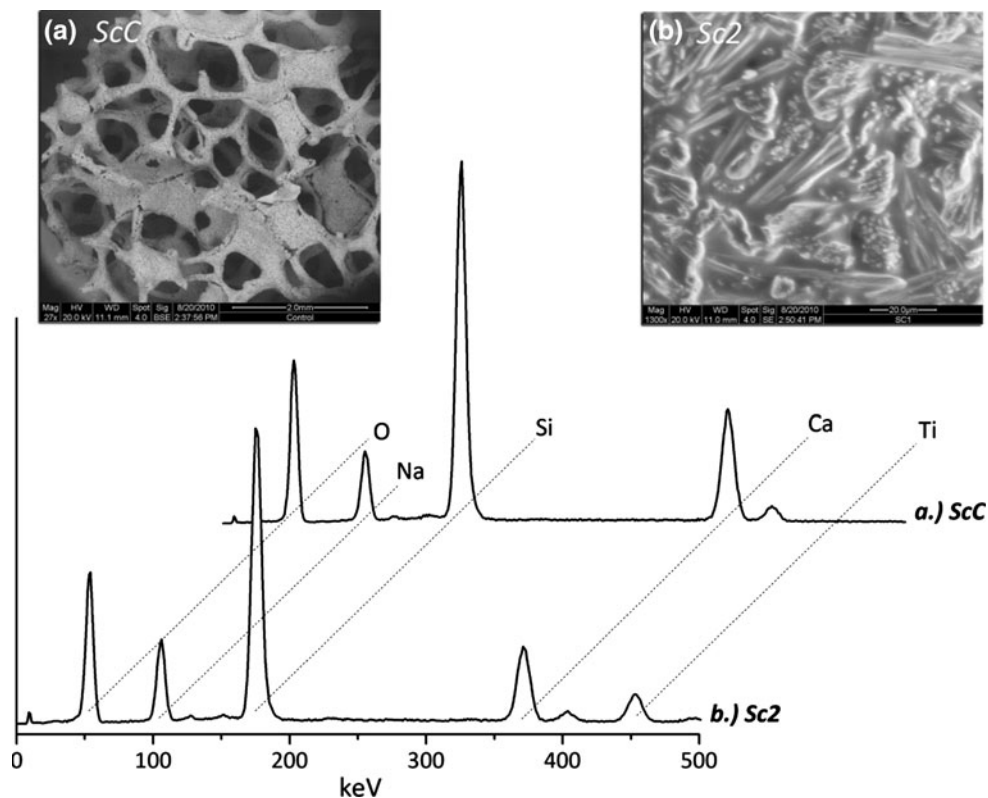**Fig. 7** SEM and EDX analysis of *ScC* and *Sc2* scaffolds

Fig. 8 Optical microscopy of pores from each material

has been cited in the literature as a preferential attribute for scaffold fabrication [4, 29, 30] as the porosity of trabecular bone is cited in the range of 80–90 % [30]. The porosity of these scaffolds was quantified by surface area analysis where the *ScC* produced the highest surface area (3.3) which corresponds to the lower value determined for the porosity. *Sc1* and *Sc2* show a lower surface area of 2.5 and 2.8, respectively, which can also be attributed to the higher degree of porosity experienced by these materials.

Structural analysis of the scaffolds determined that a higher degree of porosity and a smaller pore diameter is found with the higher Ti-containing scaffold, *Sc2*. This may serve as a positive attribute as smaller pores coupled with higher porosity may facilitate increased proliferation of cells in vivo.

In order to determine the bioactivity of these materials, each scaffold was subjected to cytotoxicity testing using mesenchymal stem cells (MSC) in order to determine cell viability after 24 and 72 h exposure times. *ScC*, *Sc1* and *Sc2* were each able to support the attachment and proliferation of adult MSCs. To visualise this, a novel approach was used whereby MSC were derived from a transgenic mouse expressing a protein such that stem cells fluoresce intensely under UV illumination. Red MSC are clearly visible on *Sc1* and *Sc2* (Fig. 11a, b, respectively). Microscopy, however, is an inaccurate measure of

both *Sc1* and *Sc2*. The struts of the experimental scaffolds (*Sc1* and *Sc2*) become thinner, which may be attributed to the TiO$_2$ content present in the initial *Sc1* and *Sc2* glasses.

X-ray microtomography was also used to determine the porosity and relative surface area of each of the glass/ceramic scaffolds. Porosity and surface area data is presented in Fig. 10. Porosity of the *ScC* was at 87 % which is lower than both the Ti containing scaffolds at 89 % (*Sc1*) and 93 % (*Sc2*). A high degree of porosity (>90 %)
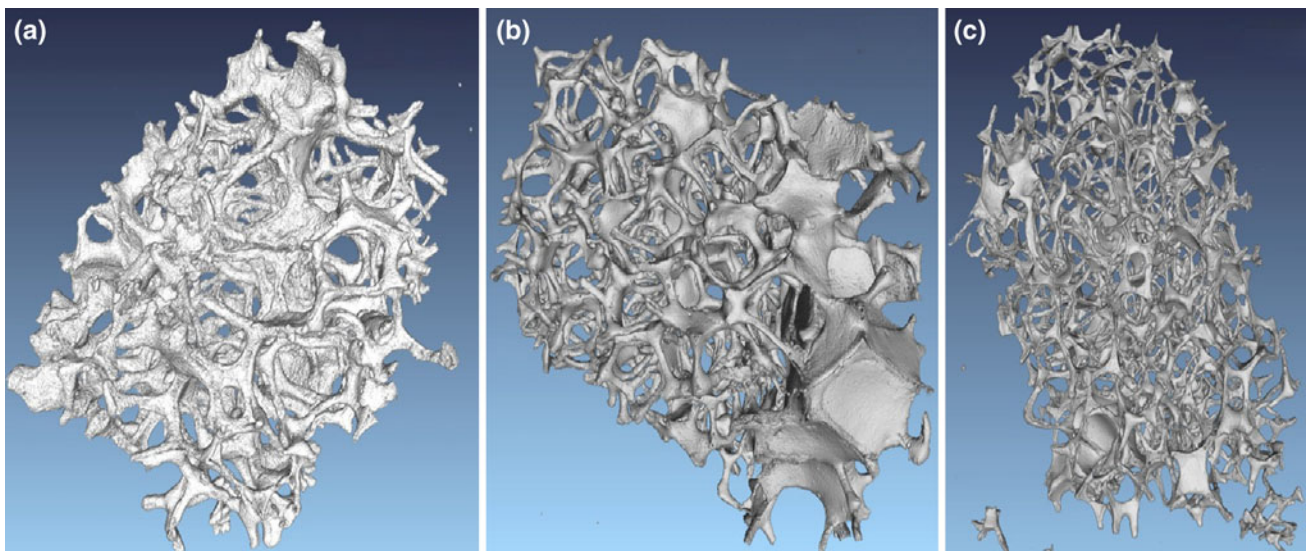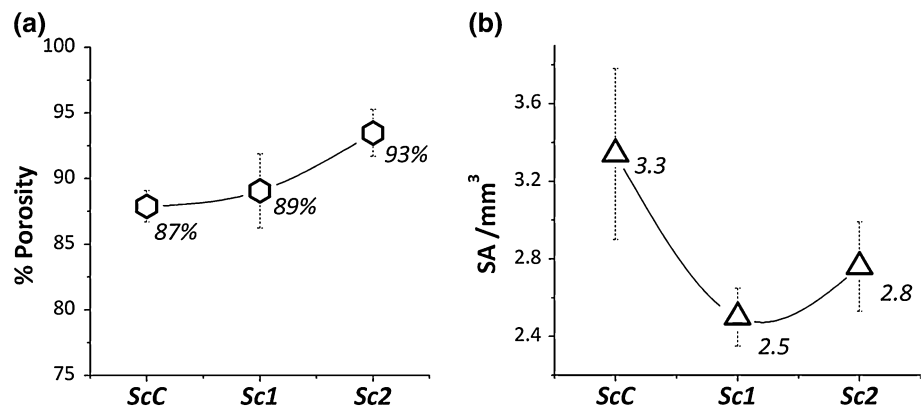
Fig. 9 X-ray microtomography imaging of **a** ScC, **b** Sc1 and **c** Sc2

Fig. 10 **a** Porosity and **b** surface area of scaffolds

viability or proliferation as cells may colonise scaffold surfaces not visible by microscopy. The nature of glass scaffolds render them unsuitable to tissue sectioning approaches as well. Therefore a biochemical assay was used which correlates to cell proliferation. Figure 11c shows that MSC colonised all scaffolds well and that MSC numbers increased over the 24 to 72 h culture period, which was particularly evident regarding the Ti-containing scaffolds.

The greatest number of viable cells was supported by *Sc2* at 72 h. Previous work suggests stem cell seeded scaffolds promote local cell function by the stem cell differentiation and also enables the scaffold surface to mimic complex local biological functions [31]. Stem cell colonisation of the scaffolds presented here is a positive attribute as it leads to the possibility of developing a stem cell seeded scaffold for bone augmentation.

To conclude, a series of glass/ceramic scaffolds were produced with TiO_2 content increasing at the expense of SiO_2. The higher TiO_2 containing scaffolds were found to have a higher degree of crystallinity at the sintering temperature which may be attributed to the higher hardness value found. The higher TiO_2 containing materials also had a smaller mean pore diameter and higher level of porosity. Bioactivity testing determined these materials to encourage the growth of mesenchymal stem cells from 24 to 72 h, which was particularly evident with the higher Ti-containing scaffold, *Sc2*. This study suggests that Ti-substituted for Si may provide a beneficial structural and therapeutic effect when fabricating glass/ceramic scaffolds for bone augmentation. Future work on these materials will include ion release studies and bioactivity testing using SBF in order to determine if the scaffolds form any carbonate hydroxyapatite surface layer.
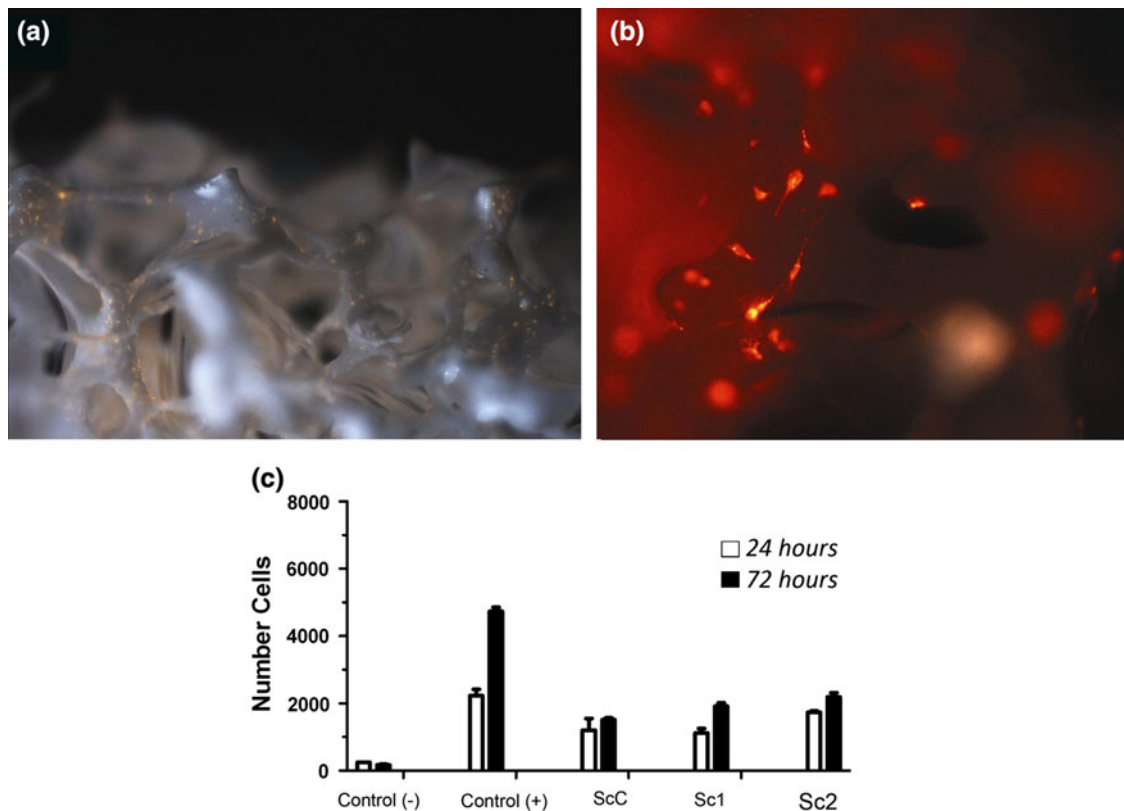
Fig. 11 MSC expressing DsRed fluorescent protein after 72 h culture on **a** *Sc1* (epi-fluorescent illumination, ×10), **b** *Sc2* (fluorescent illumination, ×40), **c** The proliferation of viable MSC on *ScC*, *Sc1* or *Sc2* was compared by WST-1 assay with *ScC* seeded by PBS alone (control−), or 3T3 fibroblast cells (control +)

References

1. Shih CJ, Chen HT, Huang LF, Lu PS, Chang HF, Chang IL. Synthesis and in vitro bioactivity of mesoporous bioactive glass scaffolds. Mater Sci Eng: C. 2010;30:657–63.
2. Zhu Y, Wu C, Ramaswamy Y, Kockrick E, Simon P, Kaskel S, Zreiqat H. Preparation, characterization and in vitro bioactivity of mesoporous bioactive glasses (MBGs) scaffolds for bone tissue engineering. Micropor Mesopor Mater. 2008;112:494–503.
3. Zhu Y, Kaskel S. Comparison of the in vitro bioactivity and drug release property of mesoporous bioactive glasses (MBGs) and bioactive glasses (BGs) scaffolds. Micropor Mesopor Mater. 2009;118:176–82.
4. Chen QZ, Thompson ID, Boccaccini AR. 45S5 Bioglass®-derived glass-ceramic scaffolds for bone tissue engineering. Biomaterials. 2006;27:2414–25.
5. Jones JR. New trends in bioactive scaffolds: the importance of nanostructure. J Eur Ceram Soc. 2009;29:1275–81.
6. Chen Q-Z, Rezwan K, Françon V, Armitage D, Nazhat SN, Jones FH, Boccaccini AR. Surface functionalization of Bioglass®-derived porous scaffolds. Acta Biomater. 2007;3:551–62.
7. Cao B, Zhou D, Xue M, Li G, Yang W, Long Q, Ji L. Study on surface modification of porous apatite-wollastonite bioactive glass ceramic scaffold. Appl Surf Sci. 2008;255:505–8.
8. Charles-Harris M, del Valle S, Hentges E, Bleuet P, Lacroix D, Planell JA. Mechanical and structural characterisation of completely degradable polylactic acid/calcium phosphate glass scaffolds. Biomaterials. 2007;28:4429–38.
9. Wren AW, Laffir FR, Kidari A, Towler MR. The structural role of titanium in Ca–Sr–Zn–Si/Ti glasses for medical applications. J Non-Crys Solids. 2010;357(3):1021–6.
10. Lausmaa J. Surface spectroscopic characterization of titanium implant materials. J Electron Spectr Related Phenom. 1996;81:343–61.
11. Schwager K. Titanium as a biomaterial for ossicular replacement: results after implantation in the middle ear of the rabbit. Eur Arch Otorhinolaryngol. 1998;255:396–401.
12. Yammamoto O, Alvarez K, Kikuchi T, Fukuda M. Fabrication and characterization of oxygen-diffused titanium for biomedical applications. Acta Biomater. 2009;5(9):3605–15.
13. Barrere F, Snel MME, van Blitterswijk CA, de Groot K, Layrolle P. Nano-scale of the nucleation and growth of calcium phosphate coating on titanium implants. Biomaterials. 2004;25:2901–10.
14. Takadama H, Kim H-M, Kokubo T, Nakamura T. XPS study of the process of apatite formation on bioactive Ti–6Al–4V alloy in simulated body fluid. Sci Technol Adv Mater. 2001;2:389–96.
15. Piscanec S, Ciacchi LC, Vesselli E, Comelli G, Sbaizero O, Meriani S, De Vita A. Bioactivity of TiN-coated titanium implants. Acta Mater. 2004;52:1237–45.
16. Kokubo T, Kim H-M, Kawashita M. Novel bioactive materials with different mechanical properties. Biomaterials. 2003;24:2161–75.
17. Kokubo T, Takadama H. How useful is SBF in predicting in vivo bone bioactivity. Biomaterials. 2006;27:2907–15.
18. Misture ST. Large-volume atmosphere-controlled diffraction furnace. Meas Sci Technol. 2003;14:1091–8.

19. Vintersten K, Monetti C, Gertsenstein M, Zhang P, Laszlo L, Biechele S, Nagy A. Mouse in red: red fluorescent protein expression in mouse ES cells, embryos, and adult animals. Genesis. 2004;40:241–6.

20. English K, Barry FP, Field-Corbett CP, Mahon BP. IFN-gamma and TNF-alpha differentially regulate immunomodulation by murine mesenchymal stem cells. Immunol Lett. 2007;110:91–100.

21. Kavanagh H, Mahon BP. Allogeneic mesenchymal stem cells prevent allergic airway inflammation by inducing murine regulatory T cells. Allergy. 2011;66(4):523–31.

22. Vargas GE, Mesones RV, Bretcanu O, López JMP, Boccaccini AR, Gorustovich A. Biocompatibility and bone mineralization potential of 45S5 Bioglass®-derived glass-ceramic scaffolds in chick embryos. Acta Biomater. 2009;5:374–80.

23. Baino F, Verné E, Vitale-Brovarone C. 3-D high-strength glass-ceramic scaffolds containing fluoroapatite for load-bearing bone portions replacement. Mater Sci Eng: C. 2009;29:2055–62.

24. Bellucci D, Cannillo V, Sola A. A new potassium-based bioactive glass: sintering behaviour and possible applications for bioceramic scaffolds. Ceram Int. 2011;37(1):145–57.

25. Huang R, Pan J, Boccaccini AR, Chen QZ. A two-scale model for simultaneous sintering and crystallization of glass-ceramic scaffolds for tissue engineering. Acta Biomater. 2008;4:1095–103.

26. Jones JR, Ehrenfried LM, Hench LL. Optimising bioactive glass scaffolds for bone tissue engineering. Biomaterials. 2006;27: 964–73.

27. Fu H, Fu Q, Zhou N, Huang W, Rahaman MN, Wang D, Liu X. In vitro evaluation of borate-based bioactive glass scaffolds prepared by a polymer foam replication method. Mater Sci Eng: C. 2009;29:2275–81.

28. Cannillo V, Chiellini F, Fabbri P, Sola A. Production of Bioglass® 45S5—polycaprolactone composite scaffolds via salt-leaching. Comp Struct. 2010;92:1823–32.

29. Esfahani SIR, Tavangarian F, Emadi R. Nanostructured bioactive glass coating on porous hydroxyapatite scaffold for strength enhancement. Mater Lett. 2008;62:3428–30.

30. Ochoa I, Sanz-Herrera JA, García-Aznar JM, Doblaré M, Yunos DM, Boccaccini AR. Permeability evaluation of 45S5 Bioglass®-based scaffolds for bone tissue engineering. J Biomech. 2009; 42:257–60.

31. Rezwan K, Chen QZ, Blaker JJ, Boccaccini AR. Biodegradable and bioactive porous polymer/inorganic composite scaffolds for bone tissue engineering. Biomaterials. 2006;27:3413–31.